Published for SISSA by Springer

Received: *February 6, 2024*
Accepted: *March 4, 2024*
Published: *April 17, 2024*

Double parton distributions with flavor interference from lattice QCD

Daniel Reitinger[a], **Christian Zimmermann**[b], **Markus Diehl**[c] **and Andreas Schäfer**[a]

[a] *Institute for Theoretical Physics, University of Regensburg, 93040 Regensburg, Germany*
[b] *Aix Marseille Univ, Université de Toulon, CNRS, CPT, Marseille, France*
[c] *Deutsches Elektronen-Synchrotron DESY, Notkestr. 85, 22607 Hamburg, Germany*

E-mail: daniel.reitinger@ur.de, christian.zimmermann@univ-amu.fr, markus.diehl@desy.de, andreas.schaefer@physik.uni-regensburg.de

Abstract: We study double parton distributions with flavor interference in the nucleon and compare them with previous results for the flavor diagonal case. We investigate both unpolarized and polarized partons. We compare our lattice results with those obtained from the simple description of the proton in terms of an SU(6) symmetric three-quark wave function and find that this description fails for both flavor and polarization dependence. We also derive and test a factorization ansatz for the unpolarized flavor interference distribution in terms of single-parton distributions and find that this ansatz fails to a large extent.

Keywords: Lattice QCD, Parton Distributions, Correlation Functions, Hadronic Spectroscopy, Structure and Interactions

ArXiv ePrint: 2401.14855

https://doi.org/10.1007/JHEP04(2024)087

Contents

1 Introduction

The Standard Model of particle physics has been extremely successful in describing experimental data at high energies. As part of this, the fundamental QCD Lagrangian has been established beyond any reasonable doubt. However, many aspects of the resulting hadron properties are still only poorly understood, e.g. the entanglement of two partons in the wave functions of a proton. Work on this front is not only motivated by the goal to better understand the strong interaction, but also by the fact that QCD effects often limit the sensitivity of searches for physics beyond the Standard Model.

An intriguing phenomenon in hadron collisions is double parton scattering (DPS), a mechanism in which two partons in each hadron take part in a hard scattering subprocess. Building on pioneering work from the 1970s and 1980s [1–7], substantial progress has been made during the last decade in an effort to develop a systematic description of DPS in QCD [8–20]. Experimental investigations of DPS started in the 1980s [21] and were followed by a wealth of studies at the Tevatron and the LHC, see for instance [22–25] and [26–32].

A crucial input for computing DPS are double parton distributions (DPDs), which describe the joint distribution of two partons inside a hadron. They quantify several types of two-particle correlations in the proton wave function and are not well known. It is natural to explore to which extent lattice QCD calculations can provide guidance in this context. In two previous publications [33, 34], we presented lattice computations of two-current correlation functions that can be related with the Mellin moments of DPDs [12]. This generalizes the well-known relation between single-current matrix elements and the Mellin moments of single-parton distributions, which has been extensively studied in the literature [37]. More recently, it has been proposed in [38, 39] to study the full functional dependence of DPDs on the lattice in the LaMET approach [40, 41]. It will be very interesting to see to which extent this can be done in practice.

JHEP04(2024)087

One should bear in mind that neither of these lattice approaches is sensitive to parton momentum fractions smaller than, say, 10^{-2}, which are responsible for much of the phase space where DPS is observed. (The same holds for quark models, which have been used extensively to compute DPDs [42–53].) However, partons with larger momentum fractions at low resolution scales are the "seeds" of evolution and thus have an imprint on partons with smaller momentum fractions at high scales. At high scales, large parton momentum fractions are probed in the production of heavy particles and thus of interest in searches for new physics. Moreover, larger parton momentum fractions become relevant when the products of the two hard scatters in DPS have a large rapidity separation. This is an interesting kinematic region, where DPS is often appreciable compared to single hard scattering. Finally, DPDs at larger momentum fractions are of interest in their own right from the point of view of exploring hadron structure.

With this in mind, we complement in the present paper our previous study [34] of DPDs in the nucleon. Specifically, we investigate flavor interference DPDs, which are characterized by different flavors for the quark (or antiquark) initiating a specific hard scattering in the amplitude and in its complex conjugate. Such distributions contribute for instance to the double Drell-Yan process. They were introduced in [12], were it was also pointed out that they do not mix with gluons under evolution, such that at small momentum fractions one can expect them to be small compared with flavor diagonal DPDs. At moderate or large momentum fractions (which are relevant for Mellin moments) there is however no argument that flavor interference should be suppressed. We will investigate whether this is the case by comparing the corresponding two-current matrix elements computed on the lattice. We will furthermore compare our lattice results (both for the flavor diagonal and the interference case) with the predictions obtained from an SU(6) symmetric three-quark wave function of the proton.

Our paper is organized as follows. In section 2, we review the different quantities relevant to our study and explain how they are related to each other. Details of the lattice setup we use are given in 3. Sections 4 and 5 contain the results of our calculations. In section 4, the Mellin moments for different combinations of flavor and polarization are presented and compared with the SU(6) predictions. In section 5 we explore to which extent DPDs can be factorized in terms of single-parton distributions. We summarize our findings in section 6.

2 Theory background

2.1 Definitions and properties

In the following, we review some basic definitions and properties of double parton distributions in the context of our lattice simulation. For more details the reader is referred to [33, 34]. DPDs describe the joint probability of finding two quarks with given polarization in a hadron. In this work we focus on the proton. We average over its polarization λ, which is indicated by the notation $\sum_\lambda' = \frac{1}{2}\sum_\lambda$. The definition of DPDs is given by

$$F_{a_1 a_2}(x_1, x_2, \boldsymbol{y}) = 2p^+ \int \mathrm{d}y^- \int \frac{\mathrm{d}z_1^-}{2\pi} \frac{\mathrm{d}z_2^-}{2\pi} e^{i(x_1 z_1^- + x_2 z_2^-)p^+} \times \sum_\lambda{}' \langle p,\lambda | \mathcal{O}_{a_1}(y, z_1)\, \mathcal{O}_{a_2}(0, z_2) | p,\lambda \rangle \,, \tag{2.1}$$

JHEP04(2024)087

where we use light-cone coordinates $v^\pm := (v^0 \pm v^3)/\sqrt{2}$ and $\boldsymbol{v} := (v^1, v^2)$ for a given four-vector v^μ. The light-cone operators are defined as

$$\mathcal{O}_a(y,z) = \bar{q}(y - \tfrac{1}{2}z)\,\Gamma_a\,q(y + \tfrac{1}{2}z)\Big|_{z^+=y^+=0,\,\boldsymbol{z}=\boldsymbol{0}}\,, \tag{2.2}$$

where a specifies the quark flavor and polarization, which is determined by the spin projections

$$\Gamma_q = \tfrac{1}{2}\gamma^+\,, \qquad \Gamma_{\Delta q} = \tfrac{1}{2}\gamma^+\gamma_5\,, \qquad \Gamma^j_{\delta q} = \tfrac{1}{2}i\sigma^{j+}\gamma_5 \quad (j=1,2)\,. \tag{2.3}$$

q refers to an unpolarized quark, Δq to a longitudinally polarized quark and δq to a transversely polarized quark. The DPDs (2.1) can be decomposed in terms of rotationally invariant functions:

$$\begin{aligned}
F_{q_1q_2}(x_1,x_2,\boldsymbol{y}) &= f_{q_1q_2}(x_1,x_2,y^2)\,,\\
F_{\Delta q_1\Delta q_2}(x_1,x_2,\boldsymbol{y}) &= f_{\Delta q_1\Delta q_2}(x_1,x_2,y^2)\,,\\
F^{j_1}_{\delta q_1 q_2}(x_1,x_2,\boldsymbol{y}) &= \epsilon^{j_1k}\boldsymbol{y}^k\,m f_{\delta q_1 q_2}(x_1,x_2,y^2)\,,\\
F^{j_2}_{q_1\delta q_2}(x_1,x_2,\boldsymbol{y}) &= \epsilon^{j_2k}\boldsymbol{y}^k\,m f_{q_1\delta q_2}(x_1,x_2,y^2)\,,\\
F^{j_1j_2}_{\delta q_1\delta q_2}(x_1,x_2,\boldsymbol{y}) &= \delta^{j_1j_2} f_{\delta q_1\delta q_2}(x_1,x_2,y^2)\\
&\quad + (2\boldsymbol{y}^{j_1}\boldsymbol{y}^{j_2} - \delta^{j_1j_2}\boldsymbol{y}^2)\,m^2 f^t_{\delta q_1\delta q_2}(x_1,x_2,y^2)\,,
\end{aligned} \tag{2.4}$$

where m denotes the proton mass and ϵ^{jk} is the antisymmetric tensor in two dimensions ($\epsilon^{12} = 1$). The definitions given above can be extended for the case of flavor-changing operators, i.e. (2.2) is modified so that the quark field has a different quark flavor than the conjugate quark field, $q \neq q'$:

$$\mathcal{O}_a(y,z) = \bar{q}(y - \tfrac{1}{2}z)\,\Gamma_a\,q'(y + \tfrac{1}{2}z)\Big|_{z^+=y^+=0,\,\boldsymbol{z}=\boldsymbol{0}}\,, \tag{2.5}$$

with $a = (qq'), \Delta(qq'), \delta(qq')$. The corresponding functions $F_{a_1a_2}(x_1,x_2,\boldsymbol{y})$ given by inserting the operators (2.5) in (2.1) are called flavor interference distributions or flavor interference DPDs. For instance, an interference contribution to the unpolarized channel is given by $F_{(ud)(du)}$, which corresponds to the operator combination $\mathcal{O}_{(ud)}\mathcal{O}_{(du)}$. Notice that in contrast to flavor diagonal DPDs, these interference DPDs cannot be interpreted as parton density distributions. Hence, there is no positivity constraint for them. Flavor interference DPDs are relevant in the description of double parton scattering, where they represent flavor interference contributions in the cross section. An example is shown in figure 1.

In the context of lattice calculations, it is useful to introduce so-called skewed DPDs, which are a generalization of ordinary DPDs in the sense that one introduces a difference between the momentum fractions of the quark in the wave function and in its complex conjugate. This difference is quantified by the skewness parameter ζ:

$$\begin{aligned}
F_{a_1a_2}(x_1,x_2,\zeta,\boldsymbol{y}) = 2p^+ \int \mathrm{d}y^-\, e^{-i\zeta y^- p^+} \int \frac{\mathrm{d}z_1^-}{2\pi}\,\frac{\mathrm{d}z_2^-}{2\pi}\, e^{i(x_1z_1^- + x_2z_2^-)p^+}\\
\times \sum_\lambda{}' \,\langle p,\lambda|\,\mathcal{O}_{a_1}(y,z_1)\,\mathcal{O}_{a_2}(0,z_2)\,|p,\lambda\rangle\,.
\end{aligned} \tag{2.6}$$

JHEP04(2024)087

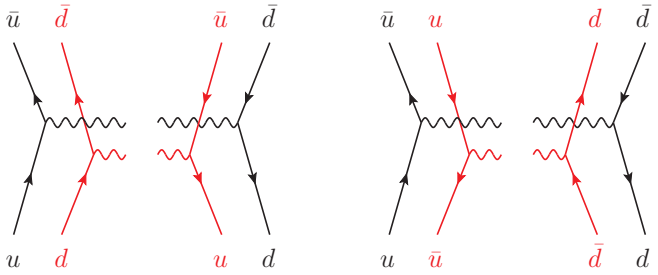

Figure 1. Example graphs for flavor interference in the double Drell-Yan process.

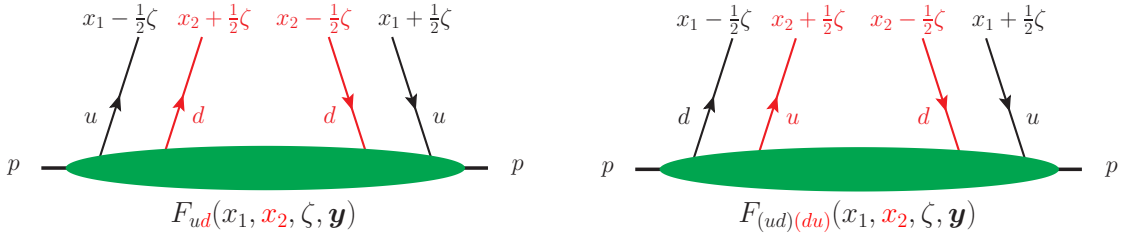

Figure 2. Skewed DPDs and their parton momentum fractions for the flavor diagonal case (left) and for flavor interference (right).

This skewed DPD has already been used in [33, 34], where also the region of support w.r.t. the parameters x_1, x_2 and ζ has been discussed in detail. Let us recall that this support region is given by:

$$|x_i \pm \tfrac{1}{2}\zeta| \leq 1\,, \qquad |x_1| + |x_2| \leq 1\,, \qquad |\zeta| \leq 1\,. \tag{2.7}$$

In figure 2 we give a graphical representation of skewed DPDs, where we indicate the longitudinal momentum fraction of the quarks in the wave function and its complex conjugate.

Moreover, we define Mellin moments w.r.t. x_1 and x_2:

$$I_{a_1 a_2}(\zeta, y^2) = \int_{-1}^{1} \mathrm{d}x_1 \int_{-1}^{1} \mathrm{d}x_2 \; f_{a_1 a_2}(x_1, x_2, \zeta, y^2)\,. \tag{2.8}$$

The symmetry properties of flavor diagonal DPDs are discussed in [34]. In the following we briefly show how these properties generalize to the flavor interference case.

For unpolarized distributions, one finds

$$\begin{aligned} f_{(ud)(du)}(x_1, x_2, \zeta, y^2) &= f_{(du)(ud)}(x_1, x_2, -\zeta, y^2)\,, \\ [f_{(ud)(du)}(x_1, x_2, \zeta, y^2)]^* &= f_{(du)(ud)}(x_1, x_2, -\zeta, y^2)\,, \\ f_{(ud)(du)}(x_1, x_2, \zeta, y^2) &= f_{(du)(ud)}(x_2, x_1, -\zeta, y^2)\,, \end{aligned} \tag{2.9}$$

where the first relation follows from PT invariance, the second one from taking the hermitian conjugate of the definition (2.6), and the third one from interchanging the two operators. From the first two relations, it follows that $f_{(ud)(du)}$ is real valued. Equations analogous to (2.9) relate $f_{\Delta(ud)\Delta(du)}$ with $f_{\Delta(du)\Delta(ud)}$, $f_{\delta(ud)\delta(du)}$ with $f_{\delta(du)\delta(ud)}$, and $f^t_{\delta(ud)\delta(du)}$ with

JHEP04(2024)087

$f^t_{\delta(du)\delta(ud)}$. For a single transverse polarization, we have instead

$$\begin{aligned} f_{(ud)\delta(du)}(x_1,x_2,\zeta,y^2) &= f_{(du)\delta(ud)}(x_1,x_2,-\zeta,y^2)\,, \\ \left[f_{(ud)\delta(du)}(x_1,x_2,\zeta,y^2)\right]^* &= f_{(du)\delta(ud)}(x_1,x_2,-\zeta,y^2)\,, \\ f_{(ud)\delta(du)}(x_1,x_2,\zeta,y^2) &= -\,f_{\delta(du)(ud)}(x_2,x_1,-\zeta,y^2)\,. \end{aligned} \tag{2.10}$$

Also in this case, we find that the distributions are real valued. Parity invariance implies that $F_{(ud)\Delta(du)}$, $F_{(du)\Delta(ud)}$, $F_{\Delta(ud)(du)}$, and $F_{\Delta(du)(ud)}$ are zero.

2.2 Euclidean matrix elements

Information about DPDs can be obtained from first principles on the lattice through Euclidean two-current matrix elements. This has been worked out in detail for the pion [33] and the nucleon [34]. In the following, we recall the important definitions and relations to DPDs and extend them to the case of flavor interference. The Euclidean two-current matrix element of the nucleon is defined as:

$$M^{\mu_1\cdots\mu_2\cdots}_{q_1q_2q_3q_4,i_1i_2}(p,y) := {\sum_\lambda}' \,\langle p,\lambda|\, J^{\mu_1\cdots}_{q_1q_2,i_1}(y)\, J^{\mu_2\cdots}_{q_3q_4,i_2}(0)\,|p,\lambda\rangle\ , \tag{2.11}$$

where we take the average of the proton spin. The currents $J^{\mu\cdots}_{qq',i}$ are local quark bilinear operators. In this work we focus on three types of currents, which are defined as:

$$J^\mu_{qq',V}(y) = \bar q(y)\gamma^\mu q'(y)\,, \quad J^\mu_{qq',A}(y) = \bar q(y)\gamma^\mu\gamma_5\, q'(y)\,, \quad J^{\mu\nu}_{qq',T}(y) = \bar q(y)\sigma^{\mu\nu}\, q'(y)\,. \tag{2.12}$$

In order to make contact with the DPDs, we decompose the matrix elements in terms of Lorentz invariant functions:

$$\begin{aligned} M^{\{\mu\nu\}}_{q_1q_2q_3q_4,VV} - \tfrac{1}{4}g^{\mu\nu}g_{\alpha\beta}M^{\alpha\beta}_{q_1q_2q_3q_4,VV} &= u^{\mu\nu}_{VV,A}\,A_{(q_1q_2)(q_3q_4)} + u^{\mu\nu}_{VV,B}\,m^2\,B_{(q_1q_2)(q_3q_4)} \\ &\quad + u^{\mu\nu}_{VV,C}\,m^4\,C_{(q_1q_2)(q_3q_4)}\,, \\ M^{\mu\nu\rho}_{q_1q_2q_3q_4,TV} + \tfrac{2}{3}g^{\rho[\mu}M^{\nu]\alpha\beta}_{q_1q_2q_3q_4,TV}g_{\alpha\beta} &= u^{\mu\nu\rho}_{TV,A}\,m\,A_{\delta(q_1q_2)(q_3q_4)} + u^{\mu\nu\rho}_{TV,B}\,m^3\,B_{\delta(q_1q_2)(q_3q_4)}\,, \\ \tfrac{1}{2}\left[M^{\mu\nu\rho\sigma}_{q_1q_2q_3q_4,TT} + M^{\rho\sigma\mu\nu}_{q_1q_2q_3q_4,TT}\right] &= \tilde u^{\mu\nu\rho\sigma}_{TT,A}\,A_{\delta(q_1q_2)\delta(q_3q_4)} + \tilde u^{\mu\nu\rho\sigma}_{TT,B}\,m^2\,B_{\delta(q_1q_2)\delta(q_3q_4)} \\ &\quad + \tilde u^{\mu\nu\rho\sigma}_{TT,C}\,m^2\,C_{\delta(q_1q_2)\delta(q_3q_4)} + \tilde u^{\mu\nu\rho\sigma}_{TT,D}\,m^4\,D_{\delta(q_1q_2)\delta(q_3q_4)} \\ &\quad + u^{\mu\nu\rho\sigma}_{TT,E}\,m^2\,\widetilde E_{\delta(q_1q_2)\delta(q_3q_4)}\,, \end{aligned} \tag{2.13}$$

where the basis tensors u and $\tilde u$, which depend on the Lorentz vectors y and p, have been defined in [34], equation (2.26). The quantities $A_{(q_1q_2)(q_3q_4)}$, etc. are Lorentz scalar functions depending only on y^2 and py. At leading twist, we only need to consider the functions $A_{(q_1q_2)(q_3q_4)}$, $A_{\Delta(q_1q_2)\Delta(q_3q_4)}$, $A_{\delta(q_1q_2)(q_3q_4)}$, $A_{(q_1q_2)\delta(q_3q_4)}$, $A_{\delta(q_1q_2)\delta(q_3q_4)}$, and $B_{\delta(q_1q_2)\delta(q_3q_4)}$. These so-called twist-two functions are directly related to the Mellin moments (2.8):

$$I_{a_1a_2}(\zeta,y^2) = \int_{-\infty}^{\infty} \mathrm{d}(py)\, e^{-i\zeta py}\, A_{a_1a_2}(py,y^2)\,, \tag{2.14}$$

$$I^t_{a_1a_2}(\zeta,y^2) = \int_{-\infty}^{\infty} \mathrm{d}(py)\, e^{-i\zeta py}\, B_{a_1a_2}(py,y^2)\,, \tag{2.15}$$

JHEP04(2024)087

where (2.15) is only defined for transverse polarization of a_1 and a_2. In this work, we shall restrict ourselves to $\vec{p} = \vec{0}$ and, therefore, $py = 0$. In this case, the twist-two functions correspond to the first moment in ζ of the DPD:

$$A_{a_1a_2}(py = 0, y^2) = \frac{1}{2\pi} \int_{-1}^{1} \mathrm{d}\zeta \, I_{a_1a_2}(\zeta, y^2) \,. \tag{2.16}$$

In [34] we found similar patterns for the twist-two functions and the reconstructed DPDs themselves regarding their dependence on the distance y and on the quark polarization.

2.3 DPDs in the SU(6) quark model

In the following, we consider a simple SU(6)-symmetric quark model and derive its predictions for matrix elements of two-quark currents. The spin-flavor part of the SU(6)-symmetric proton wave function $|p^\uparrow\rangle$ is given by:

$$\begin{aligned} |p^\uparrow\rangle = \frac{1}{3\sqrt{2}} \Big[&|u^\uparrow u^\downarrow d^\uparrow\rangle + |u^\downarrow u^\uparrow d^\uparrow\rangle - 2\,|u^\uparrow u^\uparrow d^\downarrow\rangle + |u^\uparrow d^\uparrow u^\downarrow\rangle + |u^\downarrow d^\uparrow u^\uparrow\rangle - 2\,|u^\uparrow d^\downarrow u^\uparrow\rangle + \\ &+ |d^\uparrow u^\uparrow u^\downarrow\rangle + |d^\uparrow u^\downarrow u^\uparrow\rangle - 2\,|d^\downarrow u^\uparrow u^\uparrow\rangle \Big] \,, \end{aligned} \tag{2.17}$$

where $\uparrow$ ($\downarrow$) indicates polarization along the positive (negative) z axis. Moreover, the quark operators are expressed as

$$\begin{aligned} \mathcal{O}_{(ud)} &= \frac{1}{2} \Big[(\bar{u}^\uparrow \gamma^+ d^\uparrow) + (\bar{u}^\downarrow \gamma^+ d^\downarrow) \Big] \,, \\ \mathcal{O}_{\Delta(ud)} &= \frac{1}{2} \Big[(\bar{u}^\uparrow \gamma^+ d^\uparrow) - (\bar{u}^\downarrow \gamma^+ d^\downarrow) \Big] \,, \end{aligned} \tag{2.18}$$

and likewise for the other flavor combinations. Considering matrix elements of the form $\langle p^\uparrow | \, (\bar{q}_1 \gamma^+ q_2)(\bar{q}_3 \gamma^+ q_4) \, |p^\uparrow\rangle$ for the proton state (2.17), we obtain:

$$\begin{aligned} &\langle p^\uparrow | \, (\bar{u}^\uparrow \gamma^+ u^\uparrow)(\bar{d}^\uparrow \gamma^+ d^\uparrow) \, |p^\uparrow\rangle = a \,, && \langle p^\uparrow | \, (\bar{u}^\uparrow \gamma^+ u^\uparrow)(\bar{d}^\downarrow \gamma^+ d^\downarrow) \, |p^\uparrow\rangle = 4a \,, \\ &\langle p^\uparrow | \, (\bar{u}^\downarrow \gamma^+ u^\downarrow)(\bar{d}^\uparrow \gamma^+ d^\uparrow) \, |p^\uparrow\rangle = a \,, && \langle p^\uparrow | \, (\bar{u}^\downarrow \gamma^+ u^\downarrow)(\bar{d}^\downarrow \gamma^+ d^\downarrow) \, |p^\uparrow\rangle = 0 \,, \\ &\langle p^\uparrow | \, (\bar{u}^\uparrow \gamma^+ u^\uparrow)(\bar{u}^\uparrow \gamma^+ u^\uparrow) \, |p^\uparrow\rangle = 4a \,, && \langle p^\uparrow | \, (\bar{u}^\uparrow \gamma^+ u^\uparrow)(\bar{u}^\downarrow \gamma^+ u^\downarrow) \, |p^\uparrow\rangle = a \,, \\ &\langle p^\uparrow | \, (\bar{u}^\downarrow \gamma^+ u^\downarrow)(\bar{u}^\uparrow \gamma^+ u^\uparrow) \, |p^\uparrow\rangle = a \,, && \langle p^\uparrow | \, (\bar{u}^\downarrow \gamma^+ u^\downarrow)(\bar{u}^\downarrow \gamma^+ u^\downarrow) \, |p^\uparrow\rangle = 0 \,, \\ &\langle p^\uparrow | \, (\bar{d}^\uparrow \gamma^+ u^\uparrow)(\bar{u}^\uparrow \gamma^+ d^\uparrow) \, |p^\uparrow\rangle = a \,, && \langle p^\uparrow | \, (\bar{d}^\uparrow \gamma^+ u^\uparrow)(\bar{u}^\downarrow \gamma^+ d^\downarrow) \, |p^\uparrow\rangle = -2a \,, \\ &\langle p^\uparrow | \, (\bar{d}^\downarrow \gamma^+ u^\downarrow)(\bar{u}^\uparrow \gamma^+ d^\uparrow) \, |p^\uparrow\rangle = -2a \,, && \langle p^\uparrow | \, (\bar{d}^\downarrow \gamma^+ u^\downarrow)(\bar{u}^\downarrow \gamma^+ d^\downarrow) \, |p^\uparrow\rangle = 0 \,, \end{aligned} \tag{2.19}$$

where it is understood that the four field operators are taken at different positions as specified by (2.1) and (2.2). Here the factor a depends on the orbital part of the proton wave function, which we leave unspecified. The DPDs are expressed in terms of proton matrix elements of the operators (2.18), i.e. $f_{a_1a_2} \propto \langle p^\uparrow | \, \mathcal{O}_{a_1} \mathcal{O}_{a_2} \, |p^\uparrow\rangle$. Using the results given in (2.19), we find:

$$\begin{aligned} f_{ud} &= +6\tilde{a} \,, & f_{uu} &= +6\tilde{a} \,, & f_{(du)(ud)} &= -3\tilde{a} \,, \\ f_{\Delta u \Delta d} &= -4\tilde{a} \,, & f_{\Delta u \Delta u} &= +2\tilde{a} \,, & f_{\Delta(du)\Delta(ud)} &= +5\tilde{a} \,, \end{aligned} \tag{2.20}$$

with an overall factor $\tilde{a}$ that depends again on the orbital part of the wave function. Since this orbital part is isotropic, there is no difference regarding the direction of the quark

JHEP04(2024)087

polarization. Hence, the values obtained for $f_{\Delta u \Delta d}$ are the same for $f_{\delta u \delta d}$, and likewise for all other flavor combinations. Predictions that are independent of the factor $\tilde{a}$ are obtained for *ratios* of DPDs, such as:

$$\frac{f_{(du)(ud)}}{f_{ud}} = -\frac{1}{2}\,, \qquad \frac{f_{(du)(ud)}}{f_{uu}} = -\frac{1}{2}\,, \qquad \frac{f_{ud}}{f_{uu}} = +1\,, \tag{2.21}$$

and

$$\frac{f_{\Delta(du)\Delta(ud)}}{f_{ud}} = +\frac{5}{6}\,, \qquad \frac{f_{\Delta u \Delta d}}{f_{ud}} = -\frac{2}{3}\,, \qquad \frac{f_{\Delta u \Delta u}}{f_{uu}} = +\frac{1}{3}\,. \tag{2.22}$$

Analogous predictions hold for the ratios of the twist-two functions $A_{a_1 a_2}$ and can be directly checked against lattice results.

3 Lattice calculation

In the following, we give an overview of the calculation of two-current matrix elements on the lattice and briefly review the techniques that are used. A detailed explanation is given in [34]. This shall now be extended to flavor-changing operators.

Let us first recall that the two-current matrix element (2.11) of the nucleon at $y^0 = 0$ is related to the nucleon four-point function $C_{4\mathrm{pt}}(\vec{y}, t, \tau)$ by the following formula:

$$M_{ij}(p,y)\Big|_{y^0=0} = C^{ij,\vec{p}}_{4\mathrm{pt}}(\vec{y}) := 2V\sqrt{m^2+\vec{p}^{\,2}}\;\frac{C^{ij,\vec{p}}_{4\mathrm{pt}}(\vec{y},t,\tau)}{C^{\vec{p}}_{2\mathrm{pt}}(t)}\bigg|_{0\ll\tau\ll t}\,, \tag{3.1}$$

where V is the spatial lattice volume and the four-point function $C^{ij,\vec{p}}_{4\mathrm{pt}}(\vec{y},t,\tau)$ is given by:

$$C^{ij,\vec{p}}_{4\mathrm{pt}}(\vec{y},t,\tau) := a^6 \sum_{\vec{z}',\vec{z}} e^{-i\vec{p}(\vec{z}'-\vec{z})}\;\Big\langle \mathrm{tr}\Big\{P_+\mathcal{P}(\vec{z}',t)\;J_i(\vec{y},\tau)\;J_j(\vec{0},\tau)\;\overline{\mathcal{P}}(\vec{z},0)\Big\}\Big\rangle\,. \tag{3.2}$$

Here $P_+ = (\mathbb{1}+\gamma_4)/2$ projects onto positive parity, and $\overline{\mathcal{P}}(\vec{x},t)$ and $\mathcal{P}(\vec{x},t)$ are the nucleon interpolators, for which we choose:

$$\begin{aligned}\overline{\mathcal{P}}(\vec{x},t) &:= \epsilon_{abc}\;\Big[\bar{u}_a(x)\;C\gamma_5\;\bar{d}^T_b(x)\Big]\,\bar{u}_c(x)\Big|_{x^4=t}\,,\\ \mathcal{P}(\vec{x},t) &:= \epsilon_{abc}\;u_a(x)\,\Big[u^T_b(x)\;C\gamma_5\;d_c(x)\Big]\,\Big|_{x^4=t}\,,\end{aligned} \tag{3.3}$$

where C is the charge conjugation matrix in Dirac space. The two-point function $C^{\vec{p}}_{2\mathrm{pt}}(t)$ appearing in (3.1) is defined as:

$$C^{\vec{p}}_{2\mathrm{pt}}(t) := a^6 \sum_{\vec{z}',\vec{z}} e^{-i\vec{p}(\vec{z}'-\vec{z})}\;\Big\langle \mathrm{tr}\Big\{P_+\mathcal{P}(\vec{z}',t)\;\overline{\mathcal{P}}(\vec{z},0)\Big\}\Big\rangle\,. \tag{3.4}$$

Wick contractions. The four-point function (3.2) decomposes into a definite set of Wick contractions w.r.t. the fermion fields. There are five types of contractions, which we call C_1, C_2, S_1, S_2 and D. These contractions are represented by the graphs in figure 3. Notice that, depending on the quark flavor of the operators, there are several contributions for each contraction type. For C_1-type graphs, we denote this by the flavor indices of the operator insertions $J_{q_1q_2,i}$ and $J_{q_3q_4,j}$, i.e. $C_{1,q_1q_2q_3q_4}$. For the proton, only the contractions $C_{1,uudd}$,

JHEP04(2024)087

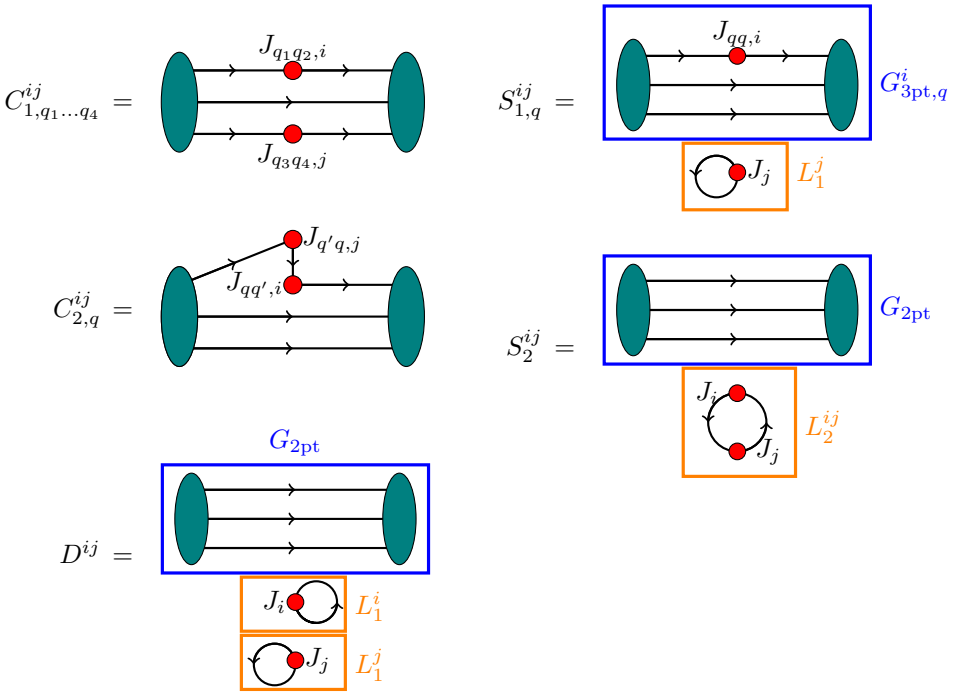

Figure 3. Depiction of the five types of Wick contractions that contribute to a nucleon four-point function. In case of C_1, C_2 and S_1 the explicit contraction depends on all involved flavors. Provided that the quark masses are taken to be equal, C_2 depends only on the flavor of the quark line that is connected to one of the insertions (red) and the source. For the disconnected diagrams S_1, S_2 and D we also indicate the disconnected parts $G_{3\mathrm{pt}}$ and $G_{2\mathrm{pt}}$ (blue), as well as the loops L_1 and L_2 (orange).

$C_{1,uuuu}$ and $C_{1,duud}$ contribute (together with $C_{1,dduu}$ and $C_{1,uddu}$, which are obtained by exchanging the two currents). In our calculation, we consider only proton matrix elements in the iso-symmetric limit, where the u-quark and the d-quark have the same mass. In that case, there are two independent contributions with C_2- or S_1-topology, namely $C_{2,u}$, $C_{2,d}$, $S_{1,u}$ and $S_{1,d}$. The indicated flavor refers to the quark line that connects one of the currents with the proton source.

The explicit set of contractions contributing to the four-point function depends on the quark flavors of the considered operators. In the following we list the decomposition of all possible matrix elements of two light-quark operators in a proton:

$$
\begin{aligned}
M_{uudd,ij}(p,y)|_{y^0=0} &= C^{ij,\vec{p}}_{1,uudd}(\vec{y}) + S^{ij,\vec{p}}_{1,u}(\vec{y}) + S^{ji,\vec{p}}_{1,d}(-\vec{y}) + D^{ij,\vec{p}}(\vec{y})\,,\\
M_{uuuu,ij}(p,y)|_{y^0=0} &= C^{ij,\vec{p}}_{1,uuuu}(\vec{y}) + C^{ij,\vec{p}}_{2,u}(\vec{y}) + C^{ji,\vec{p}}_{2,u}(-\vec{y}) + S^{ij,\vec{p}}_{1,u}(\vec{y}) + S^{ji,\vec{p}}_{1,u}(-\vec{y})\\
&\quad + S^{ij,\vec{p}}_{2}(\vec{y}) + D^{ij,\vec{p}}(\vec{y})\,,\\
M_{dddd,ij}(p,y)|_{y^0=0} &= C^{ij,\vec{p}}_{2,d}(\vec{y}) + C^{ji,\vec{p}}_{2,d}(-\vec{y}) + S^{ij,\vec{p}}_{1,d}(\vec{y}) + S^{ji,\vec{p}}_{1,d}(-\vec{y})\\
&\quad + S^{ij,\vec{p}}_{2}(\vec{y}) + D^{ij,\vec{p}}(\vec{y})\,,\\
M_{duud,ij}(p,y)|_{y^0=0} &= C^{ij,\vec{p}}_{1,duud}(\vec{y}) + C^{ij,\vec{p}}_{2,d}(\vec{y}) + C^{ji,\vec{p}}_{2,u}(-\vec{y}) + S^{ij,\vec{p}}_{2}(\vec{y})\,,\\
M_{uddu,ij}(p,y)|_{y^0=0} &= C^{ji,\vec{p}}_{1,duud}(-\vec{y}) + C^{ij,\vec{p}}_{2,u}(\vec{y}) + C^{ji,\vec{p}}_{2,d}(-\vec{y}) + S^{ij,\vec{p}}_{2}(\vec{y})\,,
\end{aligned}
\tag{3.5}
$$

JHEP04(2024)087

where we use

$$C^{ij,\vec{p}}_{1,uudd}(\vec{y}) = 2V\sqrt{m^2+\vec{p}^2}\,\frac{C^{ij,\vec{p}}_{1,uudd}(\vec{y},t,\tau)}{C^{\vec{p}}_{2\mathrm{pt}}(t)}\bigg|_{0\ll\tau\ll t} \tag{3.6}$$

and similarly for all other Wick contractions.

Renormalization. The lattice operators are renormalized multiplicatively and converted to the $\overline{\mathrm{MS}}$-scheme using the factors Z_i:

$$J_i^{\overline{\mathrm{MS}}}(y) = Z_i J_i^{\mathrm{latt}}(y)\,. \tag{3.7}$$

For $\beta = 3.4$, the corresponding values of Z_i are [54]:

$$Z_V = 0.7128\,, \qquad Z_A = 0.7525\,, \qquad Z_T = 0.8335\,, \tag{3.8}$$

for the choice

$$\mu = 2\ \mathrm{GeV}\,. \tag{3.9}$$

The renormalization of the two-current matrix elements is given by:

$$M^{\overline{\mathrm{MS}}}_{q_1q_2q_3q_4,i_1i_2} = Z_{i_1}Z_{i_2}M^{\mathrm{latt}}_{q_1q_2q_3q_4,i_1i_2}\,. \tag{3.10}$$

Technical details on Wick contractions. A sketch summarizing the techniques used to evaluate the Wick contractions is given in figure 4. The proton source is realized by a point source. Both the proton source and the proton sink are momentum smeared [55]. The corresponding smeared point-to-all propagator at the source z is denoted by $M_z^{\Phi,\vec{p}}(y)$. The contractions where at least one of the two currents is directly connected to the proton source or sink require usage of the sequential source technique. C_1 and C_2 additionally involve stochastic wall sources for a given timeslice t, for which we use $Z_2 \times Z_2$ sources. We denote the corresponding propagated stochastic source ("stochastic propagator") by $\psi_t^{(\ell)}$, where ℓ indicates the stochastic source. In the case of C_2, the stochastic source timeslice and the timeslice where the stochastic propagator is evaluated are identical. Therefore, the propagator is improved by removing terms in the corresponding hopping parameter expansion that are trivially zero in the exact case but contribute to the stochastic noise. A similar improvement is performed for the loop L_1 appearing in S_1 and D, which is also evaluated using stochastic propagators. Notice that for the D contraction we have two versions, one using stochastic sources for both loops, and one where we use point sources only for one of the two loops. More details on the techniques are given in [34]. This reference gives also explicit expressions for the quantities that are evaluated on the lattice, except for the contraction $C_{1,duud}$, which contributes only in the context of flavor interference. We find:

$$C^{ij,\vec{p}}_{1,duud}(\vec{y},t,\tau) = \frac{a^3}{N_{\mathrm{st}}}\sum_{\vec{x}}\sum_{\ell}^{N_{\mathrm{st}}}\left\langle\left[q^{T,\vec{p},(\ell)}_{2,t,j}(x)\ q^{\vec{p},(\ell)}_{1,t,i}(x+y)\right]\right\rangle\bigg|_{x^4=\tau,y^4=0} \tag{3.11}$$

with

$$\begin{aligned}\left(q^{\vec{p},(\ell)}_{1,t,i}\right)^a_\alpha(y) &:= \left(\overline{S}^{\vec{p},(\ell)}_{321,t,i}\right)^a_\alpha(y) - \left(\overline{S}^{\vec{p},(\ell)}_{123,t,i}\right)^a_\alpha(y)\,,\\ \left(q^{\vec{p},(\ell)}_{2,t,j}\right)^a_\alpha(y) &:= \left[\psi^{\dagger,(\ell)}_t(y)\ \gamma_5\Gamma_j\ M_z^{\Phi,\vec{p}}(y)\right]^a_\alpha\,,\end{aligned} \tag{3.12}$$

where $\overline{S}$ is defined in equation (A.19) of [34].

JHEP04(2024)087

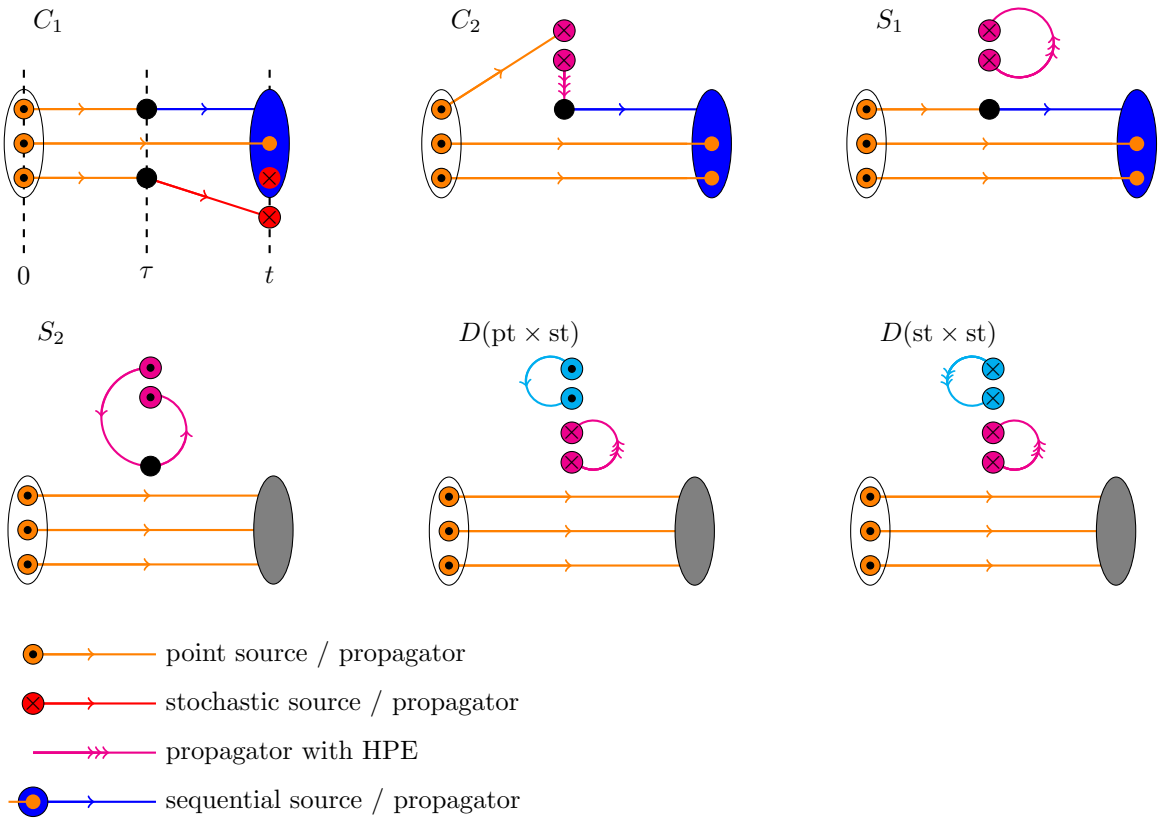

Figure 4. Sketch of all Wick contractions that are considered in this work. Colors have no meaning regarding the evaluation technique but only indicate to which source the corresponding propagator belongs. We use two evaluation methods for the D graph, which are drawn at the bottom center and the bottom right.

id	β	a[fm]	$L^3 \times T$	κ_l	κ_s	m_π[MeV]	m_K[MeV]	$m_\pi La$
H102	3.4	0.0856	$32^3 \times 96$	0.136865	0.136549339	355	441	4.9

Table 1. Details on the gauge ensemble H102, which is employed for our simulation [35, 36]. We use 990 configurations.

Lattice setup. We extend our simulation of reference [34] using the same lattice setup. In our simulation we employ the CLS ensemble H102 with $n_f = 2+1$ dynamical Sheikholeslami-Wohlert fermions [35, 36]. For completeness we list again the corresponding lattice parameters in table 1.

In addition to the contractions $C_{1,uudd}$, $C_{1,uuuu}$, $C_{2,u}$, $C_{2,d}$, $S_{1,u}$, $S_{1,d}$, S_2 and D, which have been already calculated, we compute the contraction $C_{1,duud}$ according to (3.11) for proton momentum $\vec{p} = \vec{0}$. Like for the other C_1 contractions, we choose as source-sink separation $t = 12a$ and evaluate the four-point functions for insertion times $\tau \in [3a, t - 3a]$. The corresponding data is fitted to a constant behavior in τ.

JHEP04(2024)087

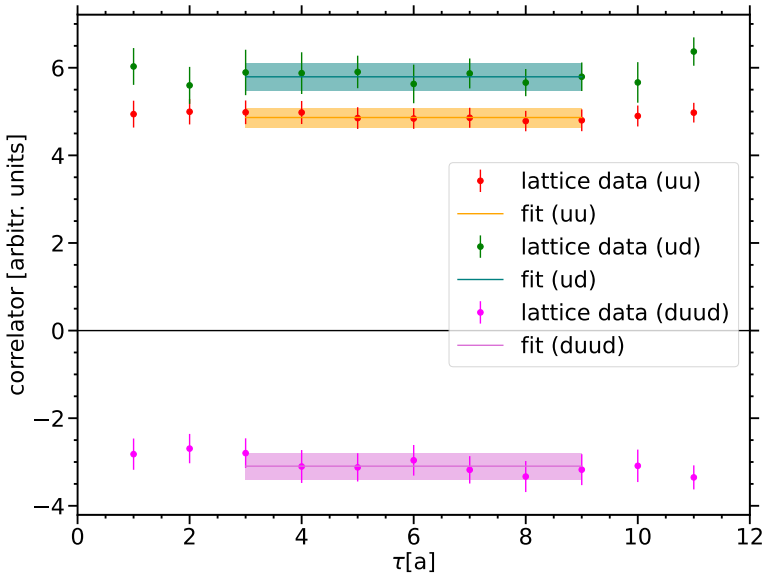

Figure 5. Dependence on the insertion time τ of the contractions $C_{1,uuuu}$ (green), $C_{1,uudd}$ (red), and $C_{1,duud}$ (magenta) for the current combination V_0V_0 and fixed quark separation $\vec{y} = (-3, 4, 3)$. The orange band represents the constant fit that returns the final value for the given $\vec{y}$.

4 Results for invariant functions

4.1 Data quality

Before we discuss our results in a physical context, we first investigate the quality of our data. In particular, we focus on the potential presence of excited states and of lattice artifacts, such as anisotropy effects. We only treat the contraction $C_{1,duud}$, since all other contributions have been already investigated in our previous work [34, 56].

Excited states. In the following we consider the τ-dependence of the four-point correlator $C_{4\text{pt}}(t, \tau, \vec{y})$ defined in (3.2) for fixed $\vec{y}$. If there is a contamination of the data by excited states, this leads to a curvature along τ. It turns out that there is in fact no visible dependence of the data on τ. As an example we show the data of the $\langle V_0V_0 \rangle$ correlator for the quark separation $\vec{y} = (-3, 4, 3)a$ in figure 5. The absence of curvature shows that excited states are sufficiently suppressed at the scale of our statistical uncertainties. The final value for the two-current correlator ground state is obtained by a constant fit in the region $3 \leq \tau \leq 9$. It has a reasonably small error and is also represented in figure 5 by the magenta band.

Anisotropy. Since we compute on a lattice with periodic boundary conditions, the effect of so-called "mirror charges" becomes important if the distance between the two current approaches half the lattice size [57, 58]. As a consequence, there are anisotropy effects whose size depends on the angle $\theta(\vec{y})$ between $\vec{y}$ and the closest diagonal of the lattice. Moreover, the lattice propagator itself exhibits anisotropy effects, which become large at small distances [59, 60]. This is the case for contractions where both operators are connected directly via a quark propagator, i.e. the C_2 and S_2 contributions. In order to reduce the violation of Lorentz invariance, only regions with $|\vec{y}| = y \geq 4a$ are considered. As discussed

JHEP04(2024)087

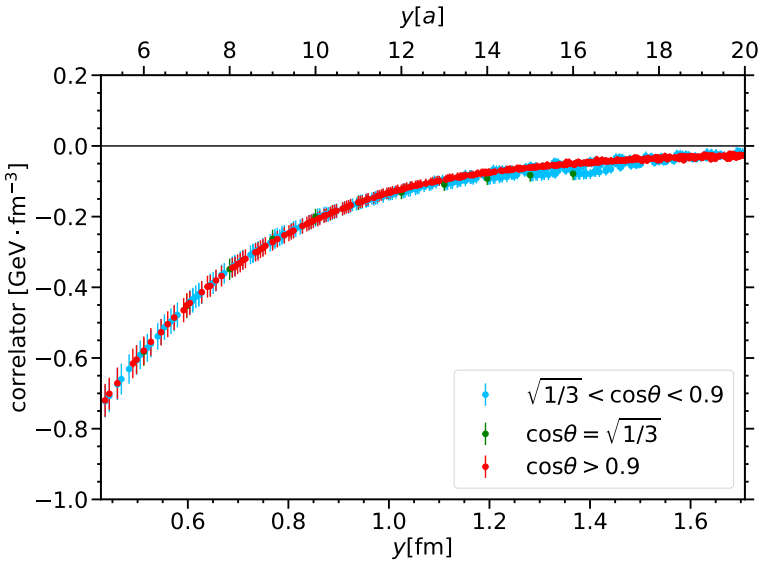

Figure 6. The anisotropy of the $C_{1,duud}$ contribution to $\langle V_0 V_0 \rangle$, revealed by a saw tooth pattern for larger angles θ between the $\vec{y}$ vector and the nearest lattice diagonal.

in section 4.1 of [34], we limit ourselves to distances $y \leq 16a$ and take into account only data points close to the lattice diagonal, in order to reduce discretization artifacts and finite volumes effects. Specifically, only data points which fulfill

$$\cos(\theta(\vec{y})) > 0.9 \tag{4.1}$$

are considered. For the contraction $C_{1,duud}$ the most important source of anisotropy is given by mirror charges, which leads to the saw tooth pattern already observed in other contractions with C_1 topology. This is illustrated in figure 6, where the data points fulfilling the constraint (4.1) are plotted in red.

4.2 Invariant functions

In the following, we consider physical matrix elements given by (3.5). We take only into account the connected contributions C_1 and C_2 for quark separations fulfilling $4a \leq y \leq 16a$ and $\cos(\theta(y)) > 0.9$. The disconnected contribution S_1 was found to be small (but noisy) compared to C_1 and C_2 in [34], whereas the errors on D were too large to make any useful statement about its size. As pointed out in [34], S_2 is seen to violate Lorentz invariance for $y < 7a$, whereas it is orders of magnitudes smaller than the other contractions for larger quark distances. For that reason, we do not take into account this contraction in our physical results. The twist-two functions $A_{a_1 a_2}$ and $B_{\delta q \delta q'}$ are obtained from the data by solving the overdetermined equation system (2.13) for momentum $\vec{p} = \vec{0}$. The system of equations is solved by χ^2-minimization (see section 3.2 of [33]). The corresponding results are shown in figure 7 for the functions $A_{qq'}$, $A_{q\delta q'}$, and $A_{\delta q \delta q'}$.[1] Here we show the results from [34] for the flavor diagonal combinations uu, ud, and dd, and compare them to our new results for the flavor interference channel. The latter are significantly different from zero and tend

[1] Our flavor generic notation q and q' for indices includes the flavor interference cases (ud) and (du).

JHEP04(2024)087

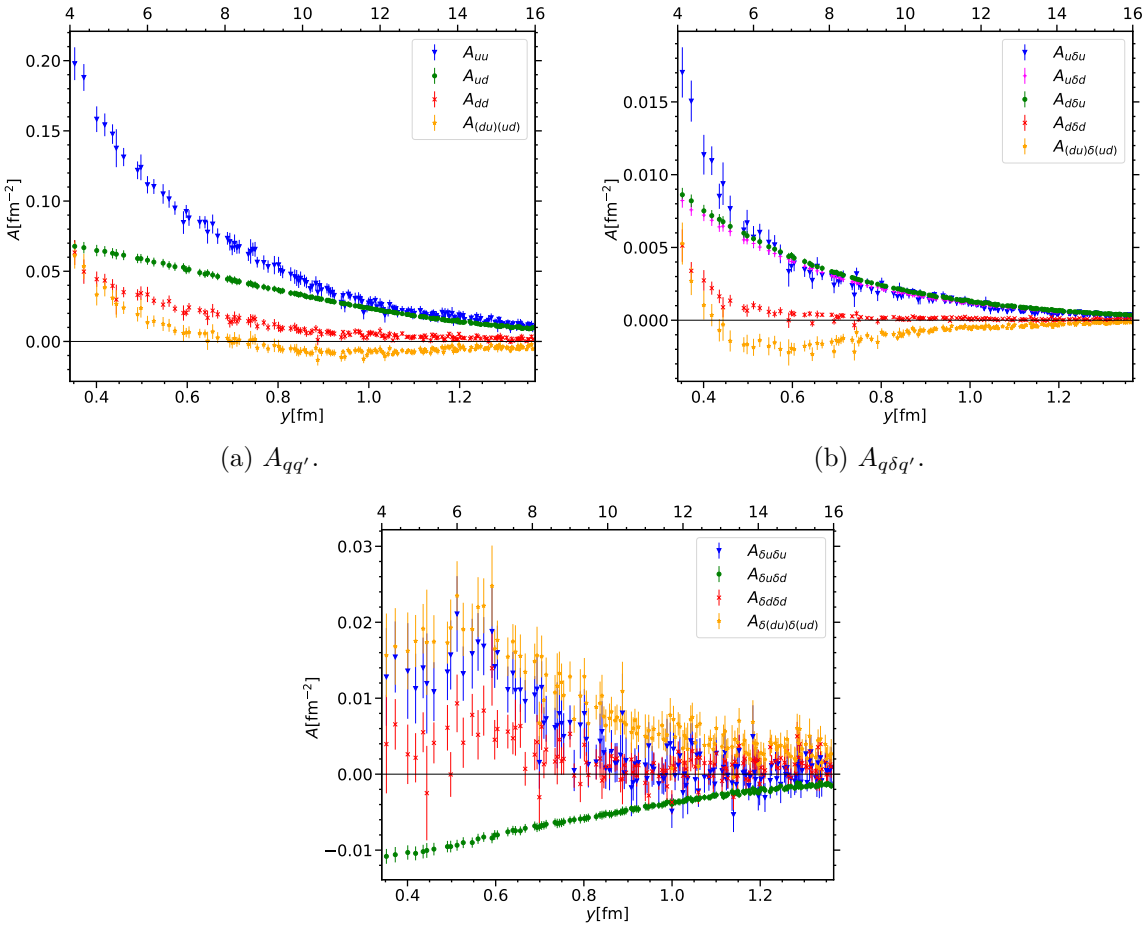

(a) $A_{qq'}$.

(b) $A_{q\delta q'}$.

(c) $A_{\delta q\delta q'}$.

Figure 7. Twist-two functions for three different polarization combinations and the flavor combinations uu, ud, dd and $(du)(ud)$. Only the graphs C_1 and C_2 are taken into account. The hadron momentum used is always zero, $\vec{p} = \vec{0}$.

to be of similar size as the dd contribution. Moreover, in the case of $A_{qq'}$ and $A_{q\delta q'}$ we observe a change in sign for the $(du)(ud)$ combination as a function of y. Hence, we can conclude that flavor interference can indeed be sizable for DPDs. We note that our results for $B_{\delta q\delta q'}$ have rather large statistical uncertainties for all flavor combinations other than ud and are hence not shown here.

4.3 Comparison with SU(6) predictions

In the following, we compare the ratios (2.21) derived for an SU(6)-symmetric three-quark wave function with the corresponding data we obtain from the lattice. Note that the evaluation of the DPDs from a three-quark wave function corresponds to the contraction C_1. whereas the interpretation of C_2 involves wave functions with additional quark-antiquark pairs, as discussed in section 4.1 of [33]. We therefore compare the SU(6) predictions with either C_1 alone, or with the sum of C_1 and C_2. This is shown in figure 8 for the unpolarized flavor ratios (2.21) and in figure 9 for the polarization ratios (2.22).

In the case of two unpolarized quarks, the SU(6) model results are fairly consistent with the corresponding C_1 results. For large quark distances y, this also holds for the sum of C_1

JHEP04(2024)087

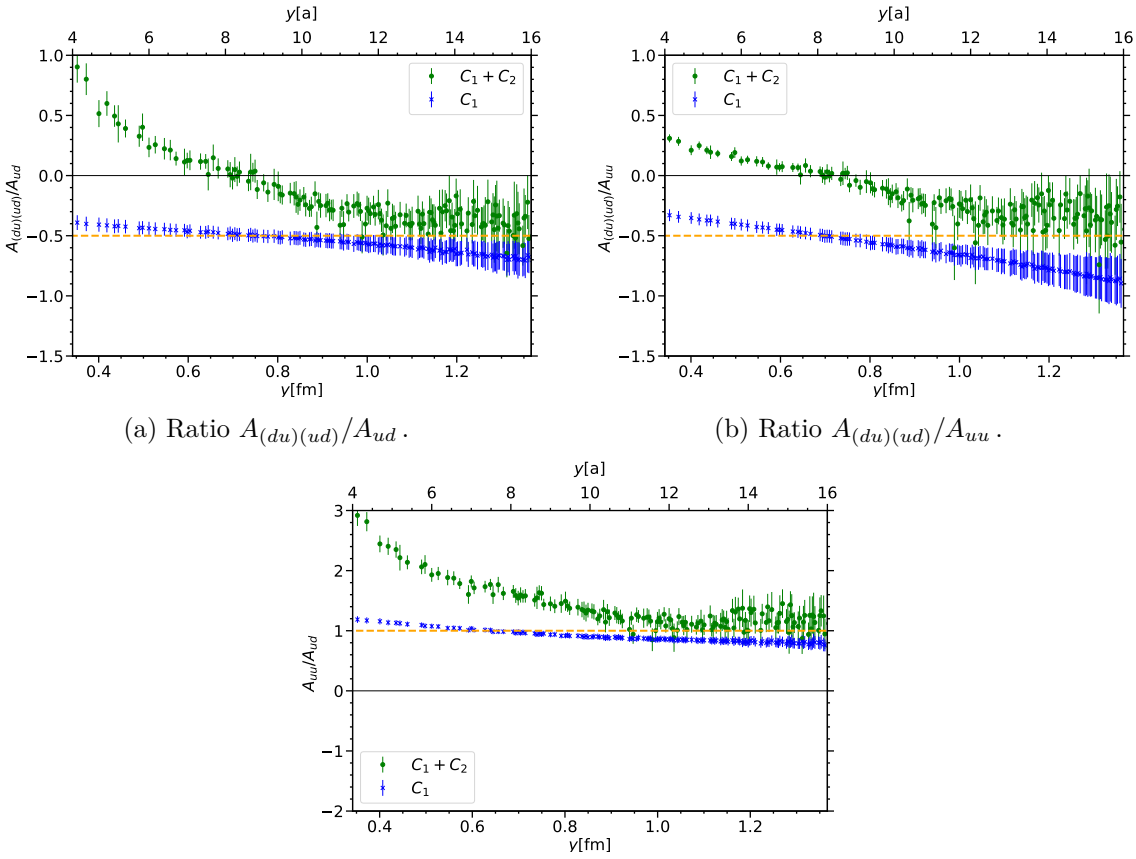

(a) Ratio $A_{(du)(ud)}/A_{ud}$.

(b) Ratio $A_{(du)(ud)}/A_{uu}$.

(c) Ratio A_{uu}/A_{ud} .

Figure 8. Ratios of unpolarized twist-two functions. The blue points correspond to only considering the C_1 graphs, and the green ones to including both C_1 and C_2 contributions. The orange dashed line is the SU(6) model prediction.

and C_2. However, for smaller y, discrepancies become rather large. By contrast, lattice results for polarization ratios, which are shown in figure 9, disagree strongly with the SU(6) model.

5 Factorization tests

A common strategy for modeling DPDs is to express them in terms of single-parton distributions, assuming that correlations between the two partons can be neglected. A corresponding ansatz can also be formulated at the level of twist-two functions [33, 34]. We now extend this formulation to the flavor interference case, which we will find to be special in this context. We limit ourselves to unpolarized quarks in the following

Technically, the factorization ansatz is obtained by inserting a complete set of eigenstates between the two operators in the DPD matrix element in (2.1) and neglecting all intermediate states except for the ground state:

$$\begin{aligned}
&\sum_{\lambda}{}' \, \langle p,\lambda |\, \mathcal{O}_{a_1}(y,z_1)\; \mathcal{O}_{a_2}(0,z_2) \,|p,\lambda\rangle \\
&\approx \sum_{\lambda,\lambda'}{}' \int \frac{\mathrm{d}p'^{+}\,\mathrm{d}^2\boldsymbol{p}'}{2p'^{+}(2\pi)^3}\, e^{-iy(p'-p)}\, \langle p,\lambda |\, \mathcal{O}_{a_1}(0,z_1) \,|p',\lambda'\rangle \, \langle p',\lambda' |\, \mathcal{O}_{a_2}(0,z_2) \,|p,\lambda\rangle \ . \qquad (5.1)
\end{aligned}$$

JHEP04(2024)087

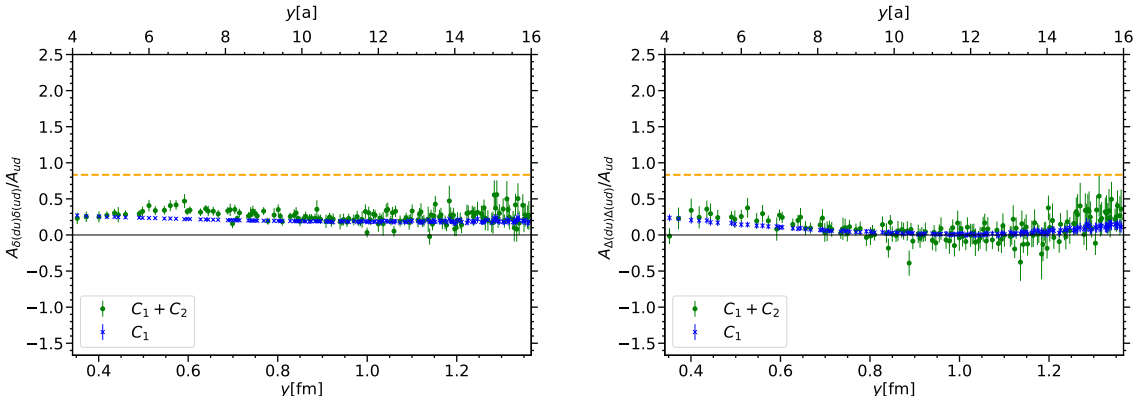

(a) Ratio $A_{\delta(du)\delta(ud)}/A_{ud}$.

(b) Ratio $A_{\Delta(du)\Delta(ud)}/A_{ud}$.

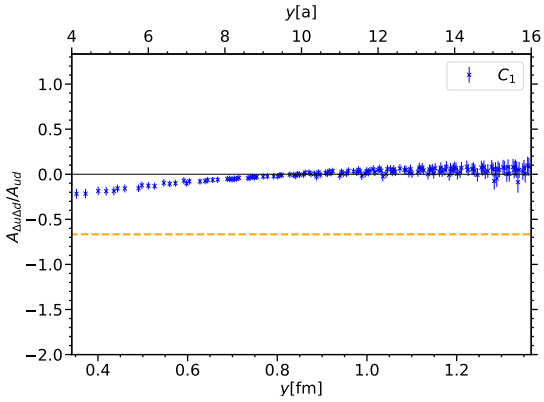

(c) Ratio $A_{\Delta u\Delta d}/A_{ud}$.

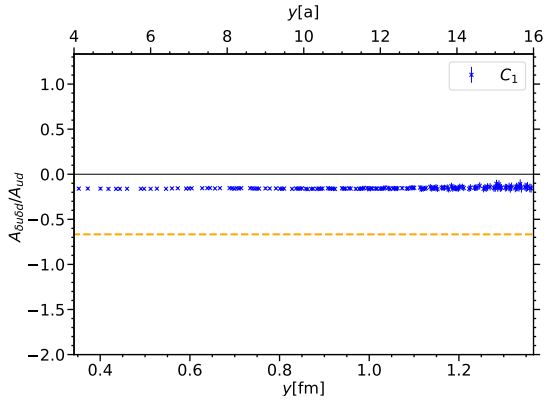

(d) Ratio $A_{\delta u\delta d}/A_{ud}$.

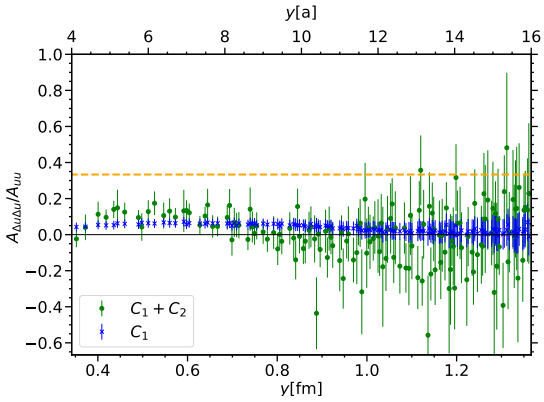

(e) Ratio $A_{\Delta u\Delta u}/A_{uu}$.

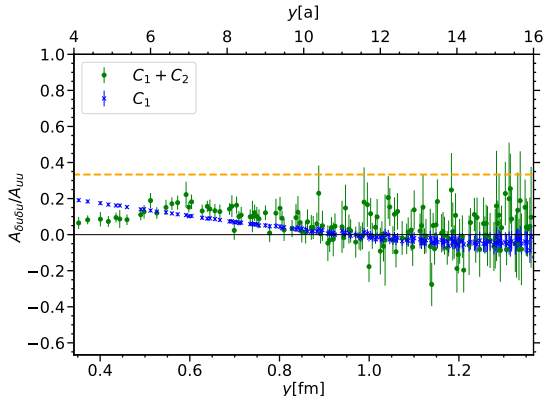

(f) Ratio $A_{\delta u\delta u}/A_{uu}$.

Figure 9. As figure 8, but for ratios of polarized and unpolarized functions. Note that there is no C_2 contribution to the flavor combination ud in panels (c) and (d).

JHEP04(2024)087

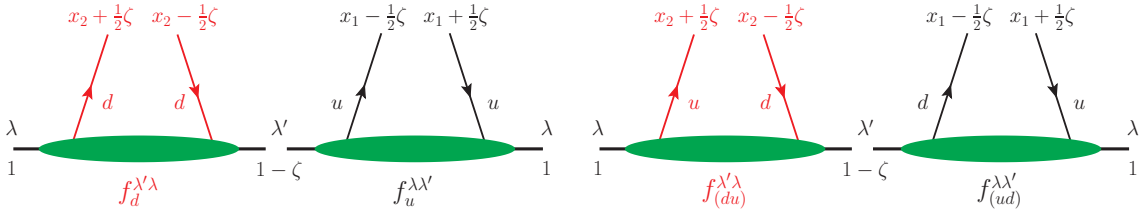

(a) F_{ud} . (b) $F_{(ud)(du)}$.

Figure 10. Depiction of the factorized expression (5.2) for the flavor-diagonal case (a), as well as the interference case (b).

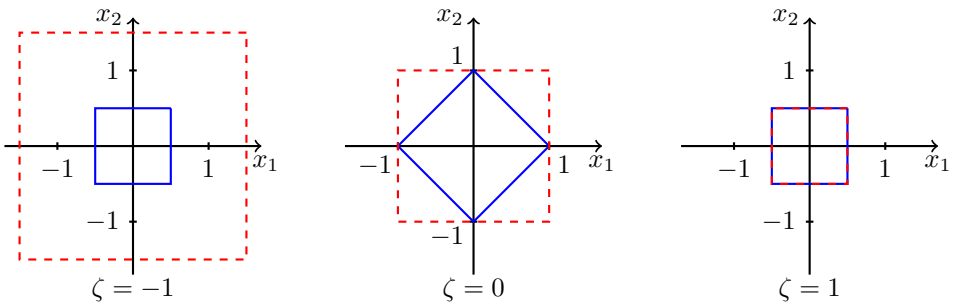

Figure 11. Support regions for different values of ζ, blue: physical support region of the DPD, red dashed: support region of the factorized expression.

In the flavor diagonal case, the matrix elements on the r.h.s. can be directly identified with GPD matrix elements $f_a^{\lambda\lambda'}(\bar{x},\xi,\boldsymbol{p}',\boldsymbol{p})$, which leads to the factorization formula for DPDs [12]:

$$F_{a_1a_2}(x_1,x_2,\zeta,\boldsymbol{y}) \stackrel{?}{=} \frac{1}{2(1-\zeta)}\int\frac{\mathrm{d}^2\boldsymbol{r}}{(2\pi)^2}\,e^{-i\boldsymbol{r}\boldsymbol{y}}\sum_{\lambda\lambda'} f_{a_1}^{\lambda\lambda'}(\bar{x}_1,-\xi,\boldsymbol{0},-\boldsymbol{r})\; f_{a_2}^{\lambda'\lambda}(\bar{x}_2,\xi,-\boldsymbol{r},\boldsymbol{0})\,, \quad (5.2)$$

where f is defined in equation (5.5) of [34]. The notation $\stackrel{?}{=}$ indicates that (5.2) is an assumption, which we investigate in the following. $\bar{x}_i$ and ξ are functions of ζ and/or x_i:

$$\bar{x}_i(x_i,\zeta) := \frac{2x_i}{2-\zeta}\,, \qquad \xi(\zeta) := \frac{\zeta}{2-\zeta}\,. \quad (5.3)$$

For flavor-changing operators, the matrix elements in the second line of (5.1) are related to GPDs for the transition between a proton and a neutron. In figure 10 we show a pictorial representation of the factorized expression in the flavor diagonal and non-diagonal cases. Using isospin symmetry, one can relate these transition GPDs to ordinary ones [61]:

$$\langle p|\,\mathcal{O}_{(ud)}\,|n\rangle = \langle p|\,\mathcal{O}_u\,|p\rangle - \langle p|\,\mathcal{O}_d\,|p\rangle = \langle n|\,\mathcal{O}_{(du)}\,|p\rangle\,, \quad (5.4)$$

which leads to the following decomposition of the flavor interference matrix element in terms of flavor conserving matrix elements:

$$\begin{aligned}\langle p|\,\mathcal{O}_{(ud)}\,|n\rangle\,\langle n|\,\mathcal{O}_{(du)}\,|p\rangle &= \Big[\langle p|\,\mathcal{O}_u\,|p\rangle - \langle p|\,\mathcal{O}_d\,|p\rangle\Big]^2 \\ &= \langle p|\,\mathcal{O}_u\,|p\rangle\,\langle p|\,\mathcal{O}_u\,|p\rangle - 2\,\langle p|\,\mathcal{O}_u\,|p\rangle\,\langle p|\,\mathcal{O}_d\,|p\rangle + \langle p|\,\mathcal{O}_d\,|p\rangle\,\langle p|\,\mathcal{O}_d\,|p\rangle\,. \end{aligned} \quad (5.5)$$

JHEP04(2024)087

Inserting this into the factorization hypothesis (5.1), we find that we can relate the flavor interference DPDs to a combination of flavor diagonal ones:

$$F_{(ud)(du)}(x_1, x_2, \zeta, \boldsymbol{y}) = F_{uu}(x_1, x_2, \zeta, \boldsymbol{y}) - 2F_{ud}(x_1, x_2, \zeta, \boldsymbol{y}) + F_{dd}(x_1, x_2, \zeta, \boldsymbol{y})\,. \tag{5.6}$$

Moreover, taking Mellin moments and performing a Fourier transform w.r.t. ζ, we find for the invariant functions:

$$A_{(ud)(du)}(py, y^2) = A_{uu}(py, y^2) - 2A_{ud}(py, y^2) + A_{dd}(py, y^2)\,. \tag{5.7}$$

Notice that the ordering of the operators is important. If we considered $\mathcal{O}_{(du)}\,\mathcal{O}_{(ud)}$ instead of $\mathcal{O}_{(ud)}\,\mathcal{O}_{(du)}$, the intermediate state with lowest energy would not be a nucleon and the corresponding transition GPDs could not be related with those in the proton. Hence, we are restricted to the operator ordering given in (5.5). In [34], we pointed out that the regions of support of the two sides of (5.2) differ to a degree that depends on the value of ζ. In particular, the mismatch is worst for $\zeta < 0$ (see figure 11). Hence, we used (5.2) only for $\zeta \geq 0$ whilst for $\zeta < 0$ we derived a factorized expression for the order $\mathcal{O}_{a_2}\mathcal{O}_{a_1}$. As we just explained, we cannot do that in the flavor interference case, where we have to keep one ordering of the operators and integrate over the entire ζ-region. This leads to:

$$\begin{aligned}
&A_{(ud)(du)}(py=0, y^2)\\
&\overset{?}{=} \frac{1}{4\pi^2}\int_{-1}^{1}\mathrm{d}\zeta\,\frac{\left(1-\frac{\zeta}{2}\right)^2}{2(1-\zeta)}\int \mathrm{d}r\; r\,J_0(yr)\sum_{\lambda\lambda'}\int \mathrm{d}x_1\;\int \mathrm{d}x_2\\
&\quad\times\Big[f_u^{\lambda\lambda'}(x_1,-\xi,\mathbf{0},-\boldsymbol{r})f_u^{\lambda'\lambda}(x_2,\xi,-\boldsymbol{r},\mathbf{0})-2f_u^{\lambda\lambda'}(x_1,-\xi,\mathbf{0},-\boldsymbol{r})f_d^{\lambda'\lambda}(x_2,\xi,-\boldsymbol{r},\mathbf{0})\\
&\qquad+f_d^{\lambda\lambda'}(x_1,-\xi,\mathbf{0},-\boldsymbol{r})f_d^{\lambda'\lambda}(x_2,\xi,-\boldsymbol{r},\mathbf{0})\Big]\,,
\end{aligned} \tag{5.8}$$

where $y = |\boldsymbol{y}|$ and $r = |\boldsymbol{r}|$. Notice that the expressions in the square brackets are rotationally invariant w.r.t. to the momentum $\boldsymbol{r}$, which allowed us to perform the angular part of the integration over $\boldsymbol{r}$. After integration over x_1 and x_2, they can be expressed in terms of Pauli and Dirac form factors, F_1 and F_2. For the second term in the square brackets of (5.8), we obtain:

$$\begin{aligned}
&\frac{1}{2}\sum_{\lambda\lambda'}\int \mathrm{d}x_1\int \mathrm{d}x_2\; f_u^{\lambda\lambda'}(x_1,-\xi,\mathbf{0},-\boldsymbol{r})\; f_d^{\lambda'\lambda}(x_2,\xi,-\boldsymbol{r},\mathbf{0})\\
&= K_1(\zeta)F_1^u(t)F_1^d(t) - K_2(\zeta)\left[F_1^u(t)F_2^d(t) + F_1^d(t)F_2^u(t)\right]\\
&\quad+\left(K_3(\zeta)+\frac{\boldsymbol{r}^2}{4m^2}K_4(\zeta)\right)F_2^u(t)F_2^d(t)\,,
\end{aligned} \tag{5.9}$$

with

$$\begin{aligned}
&t(\zeta,\boldsymbol{r}^2) := -\frac{\zeta^2m^2+\boldsymbol{r}^2}{1-\zeta}\,, && K_1(\zeta) := 1-K_2(\zeta)\,, && K_2(\zeta) := \frac{\zeta^2}{(2-\zeta)^2}\,,\\
&K_3(\zeta) := \frac{\left(K_2(\zeta)\right)^2}{K_1(\zeta)}\,, && K_4(\zeta) := \frac{1}{1-\zeta}\,.
\end{aligned} \tag{5.10}$$

Analogous expressions hold for the other terms.

JHEP04(2024)087

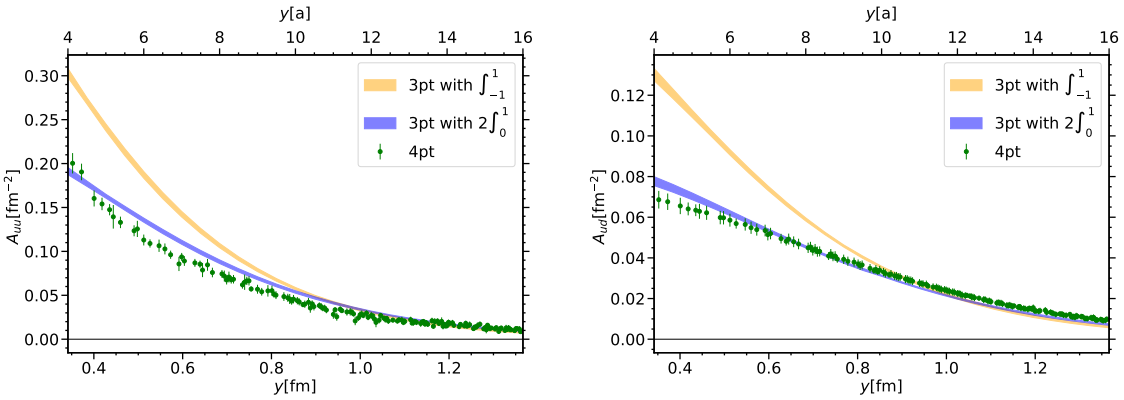

(a) $C_1 + C_2$ for flavors uu.

(b) $C_1 + C_2$ for flavors ud.

Figure 12. Factorization of the unpolarized flavor conserving twist-two functions A_{ud} and A_{uu}. The blue band shows the result for the factorization for the reduced support region that has been published in [34]. The orange band represents the factorization result where (5.2) has been directly applied without exchanging the order of operators.

For the Dirac and Pauli form factors, we take the results of lattice simulations obtained with the same ensemble used in the present work. We fitted these data to several parametrizations in [34]. In the following plots, bands correspond to the range obtained when inserting these different parametrizations into the factorization formula.

In order to check the impact of integrating (5.1) over the entire ζ-region instead of exchanging the order of operators, we repeat the factorization analysis of the flavor diagonal DPDs given in [34] by using the correspondingly modified ansatz. The result of this is shown in figure 12, along with our original result from [34], where (5.1) was only used for $\zeta \geq 0$. We see that the difference due to the increased unphysical support region is considerable when going to quark distances below about 0.8 fm. This shows that integrating (5.1) over the entire ζ-region yields a very poor approximation for small quark distances. Unfortunately, for the flavor interference contribution this is the only possibility we have found.

The result for flavor interference DPDs is plotted in figure 13 and compared to the corresponding result of the direct calculation (green). Based on the comparison in figure 13, we consider the factorization formula that uses the full ζ-region as unreliable for $y < 0.8$ fm. In the region 0.8 fm $< y <$ 1.1 fm, we observe that the factorization ansatz yields the wrong sign. The only approximate agreement with the four-point result can be observed for very large quark distances, where the result is close to zero. Hence, we conclude that within a wide range of y, the factorization ansatz is either not reliable because of the mismatch of the support regions, or it fails.

Let us finally discuss the flavor relation (5.7), which follows from our factorization formula but is more general. We see in figure 13 that the left- and right-hand sides of this relation typically differ by a factor around 2 in the full y range of the plot. The relation is thus satisfied somewhat better than the factorization hypothesis for $A_{(ud)(du)}$ in terms of three-point correlation functions.

JHEP04(2024)087

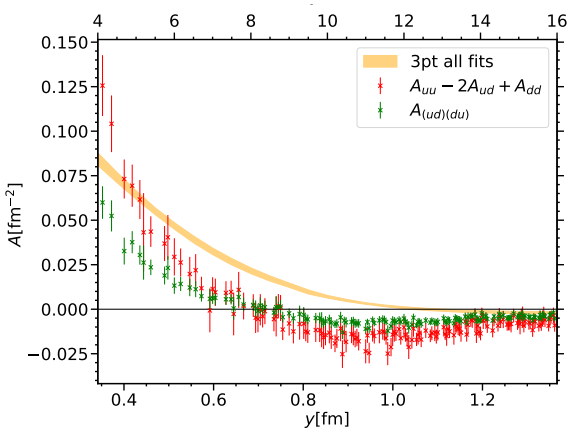

Figure 13. Factorization of the unpolarized flavor interference twist-two function $A_{(ud)(du)}$. The orange band represents the result obtained from (5.8). This is compared to the corresponding results obtained from our four-point function calculation. Here we show the data points for $A_{(ud)(du)}$ (green) and the r.h.s. of the flavor relation (5.7) (red).

6 Conclusions

We extended our work on nucleon DPDs [34] by considering flavor interference distributions. We calculated the corresponding Wick contractions and extracted the twist-two functions for the flavor combination $(ud)(du)$ for all relevant quark polarizations. This we did for zero proton momentum, which implies $py = 0$. We find that the resulting signal for flavor interference is non-negligible and of the same order of magnitude as the dd contributions. This suggests that at large parton momentum fractions, flavor interference DPDs may not be negligible.

Several relations between the different flavor and polarization combinations can be derived in a simple SU(6) quark model, which can then be compared to the corresponding lattice quantities. We observe good agreement between the lattice data and the SU(6) results for unpolarized quarks if we only take into account the contribution of the C_1 contraction, which is most consistent with the picture of a three-quark wave function. If one considers the full connected contribution $(C_1 + C_2)$ there is a significant mismatch, which increases for smaller quark distances. The SU(6) model completely fails in the case of two-parton matrix elements for polarized quarks. Finally, we considered the factorization of flavor interference DPDs in terms of GPDs. We found that, depending on the considered quark distance, the factorization ansatz is either not reliable or it does not work in the region where the signal is clearly non-zero.

Acknowledgments

This work was in part supported by the Deutsche Forschungsgemeinschaft (DFG, German Research Foundation) by project SCHA 458/23 and FOR 2926, grant number 40965613. The project leading to this publication received funding from the Excellence Initiative of Aix-Marseille University — A*MIDEX, a French "Investissements d'Avenir" programme, AMX-18-ACE-005. We gratefully acknowledge helpful discussions with Gunnar Bali. Moreover, we acknowledge the CLS effort for generating the $n_f = 2 + 1$ ensembles, one of which was used for this work.

JHEP04(2024)087

References

[1] P.V. Landshoff and J.C. Polkinghorne, *Calorimeter Triggers for Hard Collisions*, *Phys. Rev. D* **18** (1978) 3344 [INSPIRE].

[2] R. Kirschner, *Generalized Lipatov-Altarelli-Parisi Equations and Jet Calculus Rules*, *Phys. Lett. B* **84** (1979) 266 [INSPIRE].

[3] H.D. Politzer, *Power Corrections at Short Distances*, *Nucl. Phys. B* **172** (1980) 349 [INSPIRE].

[4] N. Paver and D. Treleani, *Multi-Quark Scattering and Large p_T Jet Production in Hadronic Collisions*, *Nuovo Cim. A* **70** (1982) 215 [INSPIRE].

[5] V.P. Shelest, A.M. Snigirev and G.M. Zinovev, *The Multiparton Distribution Equations in QCD*, *Phys. Lett. B* **113** (1982) 325 [INSPIRE].

[6] M. Mekhfi, *Multiparton Processes: An Application to Double Drell-Yan*, *Phys. Rev. D* **32** (1985) 2371 [INSPIRE].

[7] T. Sjostrand and M. van Zijl, *Multiple Parton-parton Interactions in an Impact Parameter Picture*, *Phys. Lett. B* **188** (1987) 149 [INSPIRE].

[8] B. Blok, Y. Dokshitzer, L. Frankfurt and M. Strikman, *The four jet production at LHC and Tevatron in QCD*, *Phys. Rev. D* **83** (2011) 071501 [arXiv:1009.2714] [INSPIRE].

[9] J.R. Gaunt and W.J. Stirling, *Double Parton Scattering Singularity in One-Loop Integrals*, *JHEP* **06** (2011) 048 [arXiv:1103.1888] [INSPIRE].

[10] M.G. Ryskin and A.M. Snigirev, *A fresh look at double parton scattering*, *Phys. Rev. D* **83** (2011) 114047 [arXiv:1103.3495] [INSPIRE].

[11] B. Blok, Y. Dokshitser, L. Frankfurt and M. Strikman, *pQCD physics of multiparton interactions*, *Eur. Phys. J. C* **72** (2012) 1963 [arXiv:1106.5533] [INSPIRE].

[12] M. Diehl, D. Ostermeier and A. Schäfer, *Elements of a theory for multiparton interactions in QCD*, *JHEP* **03** (2012) 089 [*Erratum ibid.* **03** (2016) 001] [arXiv:1111.0910] [INSPIRE].

[13] A.V. Manohar and W.J. Waalewijn, *A QCD Analysis of Double Parton Scattering: Color Correlations, Interference Effects and Evolution*, *Phys. Rev. D* **85** (2012) 114009 [arXiv:1202.3794] [INSPIRE].

[14] A.V. Manohar and W.J. Waalewijn, *What is Double Parton Scattering?*, *Phys. Lett. B* **713** (2012) 196 [arXiv:1202.5034] [INSPIRE].

[15] M.G. Ryskin and A.M. Snigirev, *Double parton scattering in double logarithm approximation of perturbative QCD*, *Phys. Rev. D* **86** (2012) 014018 [arXiv:1203.2330] [INSPIRE].

[16] J.R. Gaunt, *Single Perturbative Splitting Diagrams in Double Parton Scattering*, *JHEP* **01** (2013) 042 [arXiv:1207.0480] [INSPIRE].

[17] B. Blok, Y. Dokshitzer, L. Frankfurt and M. Strikman, *Perturbative QCD correlations in multi-parton collisions*, *Eur. Phys. J. C* **74** (2014) 2926 [arXiv:1306.3763] [INSPIRE].

[18] M. Diehl, J.R. Gaunt and K. Schönwald, *Double hard scattering without double counting*, *JHEP* **06** (2017) 083 [arXiv:1702.06486] [INSPIRE].

JHEP04(2024)087

[19] B. Cabouat, J.R. Gaunt and K. Ostrolenk, *A Monte-Carlo Simulation of Double Parton Scattering*, *JHEP* **11** (2019) 061 [arXiv:1906.04669] [INSPIRE].

[20] B. Cabouat and J.R. Gaunt, *Combining single and double parton scatterings in a parton shower*, *JHEP* **10** (2020) 012 [arXiv:2008.01442] [INSPIRE].

[21] AXIAL FIELD SPECTROMETER collaboration, *Double Parton Scattering in pp Collisions at* $\sqrt{s} = 63$*-GeV*, *Z. Phys. C* **34** (1987) 163 [INSPIRE].

[22] CDF collaboration, *Study of four jet events and evidence for double parton interactions in* $p\bar{p}$ *collisions at* $\sqrt{s} = 1.8$ *TeV*, *Phys. Rev. D* **47** (1993) 4857 [INSPIRE].

[23] CDF collaboration, *Measurement of double parton scattering in* $\bar{p}p$ *collisions at* $\sqrt{s} = 1.8$ *TeV*, *Phys. Rev. Lett.* **79** (1997) 584 [INSPIRE].

[24] D0 collaboration, *Double parton interactions in* $\gamma + 3$ *jet events in* $p\bar{p}$ *collisions* $\sqrt{s} = 1.96$ *TeV*, *Phys. Rev. D* **81** (2010) 052012 [arXiv:0912.5104] [INSPIRE].

[25] D0 collaboration, *Evidence for simultaneous production of* J/ψ *and* Υ *mesons*, *Phys. Rev. Lett.* **116** (2016) 082002 [arXiv:1511.02428] [INSPIRE].

[26] LHCB collaboration, *Observation of double charm production involving open charm in pp collisions at* $\sqrt{s} = 7$ *TeV*, *JHEP* **06** (2012) 141 [*Addendum ibid.* **03** (2014) 108] [arXiv:1205.0975] [INSPIRE].

[27] ATLAS collaboration, *Measurement of hard double-parton interactions in* $W(\rightarrow l\nu) + 2$ *jet events at* $\sqrt{s} = 7$ *TeV with the ATLAS detector*, *New J. Phys.* **15** (2013) 033038 [arXiv:1301.6872] [INSPIRE].

[28] CMS collaboration, *Study of Double Parton Scattering Using* $W + 2$*-Jet Events in Proton-Proton Collisions at* $\sqrt{s} = 7$ *TeV*, *JHEP* **03** (2014) 032 [arXiv:1312.5729] [INSPIRE].

[29] ATLAS collaboration, *Study of hard double-parton scattering in four-jet events in pp collisions at* $\sqrt{s} = 7$ *TeV with the ATLAS experiment*, *JHEP* **11** (2016) 110 [arXiv:1608.01857] [INSPIRE].

[30] LHCB collaboration, *Production of associated Y and open charm hadrons in pp collisions at* $\sqrt{s} = 7$ *and* 8 *TeV via double parton scattering*, *JHEP* **07** (2016) 052 [arXiv:1510.05949] [INSPIRE].

[31] LHCB collaboration, *Observation of Enhanced Double Parton Scattering in Proton-Lead Collisions at* $\sqrt{s_{NN}} = 8.16$ *TeV*, *Phys. Rev. Lett.* **125** (2020) 212001 [arXiv:2007.06945] [INSPIRE].

[32] CMS collaboration, *Observation of same-sign WW production from double parton scattering in proton-proton collisions at* $\sqrt{s} = 13$ *TeV*, *Phys. Rev. Lett.* **131** (2023) 091803 [arXiv:2206.02681] [INSPIRE].

[33] G.S. Bali et al., *Double parton distributions in the pion from lattice QCD*, *JHEP* **02** (2021) 067 [arXiv:2006.14826] [INSPIRE].

[34] G.S. Bali et al., *Double parton distributions in the nucleon from lattice QCD*, *JHEP* **09** (2021) 106 [arXiv:2106.03451] [INSPIRE].

[35] M. Bruno, T. Korzec and S. Schaefer, *Setting the scale for the CLS* $2 + 1$ *flavor ensembles*, *Phys. Rev. D* **95** (2017) 074504 [arXiv:1608.08900] [INSPIRE].

[36] M. Bruno et al., *Simulation of QCD with* $N_f = 2 + 1$ *flavors of non-perturbatively improved Wilson fermions*, *JHEP* **02** (2015) 043 [arXiv:1411.3982] [INSPIRE].

[37] H.-W. Lin et al., *Parton distributions and lattice QCD calculations: a community white paper*, *Prog. Part. Nucl. Phys.* **100** (2018) 107 [arXiv:1711.07916] [INSPIRE].

JHEP04(2024)087

[38] J.-H. Zhang, *Double Parton Distributions from Euclidean Lattice*, arXiv:2304.12481 [INSPIRE].

[39] M. Jaarsma, R. Rahn and W.J. Waalewijn, *Towards double parton distributions from first principles using Large Momentum Effective Theory*, *JHEP* **12** (2023) 014 [arXiv:2305.09716] [INSPIRE].

[40] X. Ji, *Parton Physics on a Euclidean Lattice*, *Phys. Rev. Lett.* **110** (2013) 262002 [arXiv:1305.1539] [INSPIRE].

[41] X. Ji et al., *Large-momentum effective theory*, *Rev. Mod. Phys.* **93** (2021) 035005 [arXiv:2004.03543] [INSPIRE].

[42] H.-M. Chang, A.V. Manohar and W.J. Waalewijn, *Double Parton Correlations in the Bag Model*, *Phys. Rev. D* **87** (2013) 034009 [arXiv:1211.3132] [INSPIRE].

[43] M. Rinaldi, S. Scopetta and V. Vento, *Double parton correlations in constituent quark models*, *Phys. Rev. D* **87** (2013) 114021 [arXiv:1302.6462] [INSPIRE].

[44] W. Broniowski and E. Ruiz Arriola, *Valence double parton distributions of the nucleon in a simple model*, *Few Body Syst.* **55** (2014) 381 [arXiv:1310.8419] [INSPIRE].

[45] M. Rinaldi, S. Scopetta, M. Traini and V. Vento, *Double parton correlations and constituent quark models: a Light Front approach to the valence sector*, *JHEP* **12** (2014) 028 [arXiv:1409.1500] [INSPIRE].

[46] W. Broniowski, E. Ruiz Arriola and K. Golec-Biernat, *Generalized Valon Model for Double Parton Distributions*, *Few Body Syst.* **57** (2016) 405 [arXiv:1602.00254] [INSPIRE].

[47] T. Kasemets and A. Mukherjee, *Quark-gluon double parton distributions in the light-front dressed quark model*, *Phys. Rev. D* **94** (2016) 074029 [arXiv:1606.05686] [INSPIRE].

[48] M. Rinaldi, S. Scopetta, M.C. Traini and V. Vento, *Correlations in Double Parton Distributions: Perturbative and Non-Perturbative effects*, *JHEP* **10** (2016) 063 [arXiv:1608.02521] [INSPIRE].

[49] M. Rinaldi and F.A. Ceccopieri, *Relativistic effects in model calculations of double parton distribution function*, *Phys. Rev. D* **95** (2017) 034040 [arXiv:1611.04793] [INSPIRE].

[50] M. Rinaldi, S. Scopetta, M. Traini and V. Vento, *A model calculation of double parton distribution functions of the pion*, *Eur. Phys. J. C* **78** (2018) 781 [arXiv:1806.10112] [INSPIRE].

[51] A. Courtoy, S. Noguera and S. Scopetta, *Double parton distributions in the pion in the Nambu-Jona-Lasinio model*, *JHEP* **12** (2019) 045 [arXiv:1909.09530] [INSPIRE].

[52] W. Broniowski and E. Ruiz Arriola, *Double parton distribution of valence quarks in the pion in chiral quark models*, *Phys. Rev. D* **101** (2020) 014019 [arXiv:1910.03707] [INSPIRE].

[53] W. Broniowski and E. Ruiz Arriola, *Double parton distributions of the pion in the NJL model*, *PoS* **LC2019** (2020) 031 [arXiv:2001.00883] [INSPIRE].

[54] RQCD collaboration, *Nonperturbative Renormalization in Lattice QCD with three Flavors of Clover Fermions: Using Periodic and Open Boundary Conditions*, *Phys. Rev. D* **103** (2021) 094511 [*Erratum ibid.* **107** (2023) 039901] [arXiv:2012.06284] [INSPIRE].

[55] G.S. Bali, B. Lang, B.U. Musch and A. Schäfer, *Novel quark smearing for hadrons with high momenta in lattice QCD*, *Phys. Rev. D* **93** (2016) 094515 [arXiv:1602.05525] [INSPIRE].

[56] RQCD collaboration, *Two-current correlations and DPDs for the nucleon on the lattice*, *PoS* **LATTICE2019** (2019) 040 [arXiv:1911.05051] [INSPIRE].

[57] M. Burkardt, J.M. Grandy and J.W. Negele, *Calculation and interpretation of hadron correlation functions in lattice QCD*, *Annals Phys.* **238** (1995) 441 [hep-lat/9406009] [INSPIRE].

JHEP04(2024)087

[58] C. Alexandrou and G. Koutsou, *A Study of Hadron Deformation in Lattice QCD*, *Phys. Rev. D* **78** (2008) 094506 [arXiv:0809.2056] [INSPIRE].

[59] G.S. Bali et al., *Pion distribution amplitude from Euclidean correlation functions: Exploring universality and higher-twist effects*, *Phys. Rev. D* **98** (2018) 094507 [arXiv:1807.06671] [INSPIRE].

[60] K. Cichy, K. Jansen and P. Korcyl, *Non-perturbative renormalization in coordinate space for $N_f = 2$ maximally twisted mass fermions with tree-level Symanzik improved gauge action*, *Nucl. Phys. B* **865** (2012) 268 [arXiv:1207.0628] [INSPIRE].

[61] L. Mankiewicz, G. Piller and T. Weigl, *Hard leptoproduction of charged vector mesons*, *Phys. Rev. D* **59** (1999) 017501 [hep-ph/9712508] [INSPIRE].

JHEP04(2024)087